ELSEVIER

Materials Science and Engineering A 457 (2007) 205–218

MATERIALS SCIENCE & ENGINEERING A

www.elsevier.com/locate/msea

A microstructural investigation of adiabatic shear bands in an interstitial free steel

J.F.C. Lins [a,*], H.R.Z. Sandim [b], H.-J. Kestenbach [c], D. Raabe [d], K.S. Vecchio [e]

[a] *Programa de Pós-graduação em Engenharia Metalúrgica, Escola de Engenharia Industrial Metalúrgica de Volta Redonda, Universidade Federal Fluminense, Volta Redonda 27255-125, Brazil*

[b] *Departamento de Engenharia de Materiais, Escola de Engenharia de Lorena, Universidade de São Paulo, Lorena 12600-970, Brazil*

[c] *Departamento de Engenharia de Materiais, Universidade Federal de São Carlos, São Carlos 13565-905, Brazil*

[d] *Max-Planck-Institut für Eisenforschung, Max-Planck-Straße 1, Düsseldorf 40237, Germany*

[e] *Department of Mechanical and Aerospace Engineering, University of California, San Diego, La Jolla, CA 92093-0411, USA*

Received 14 September 2006; received in revised form 4 December 2006; accepted 5 December 2006

Abstract

We report the microstructural characterization of induced adiabatic shear bands (ASB) in a hot-rolled interstitial free (IF) steel deformed at high strain rates (>$2.8 \times 10^4\ s^{-1}$) in a split Hopkinson bar under controlled conditions at −50 and 25 °C. Scanning electron microscopy (SEM), transmission electron microscopy (TEM) and electron backscatter diffraction (EBSD) were used to reveal the degree of subdivision within ASB and neighboring grains. Deformation twins were found in adjacent grains suggesting that twinning occurs before the flow associated to shear banding. *Progressive subgrain misorientation* (PriSM) recrystallization is a plausible mechanism to explain the development of a new structure consisting of weakly textured ultrafine grains (0.1–0.5 μm) within the ASB. Recrystallization is proposed to occur by the formation and mechanical rotation of subgrains during deformation, coupled with boundary refinement via diffusion during shear band cooling. The presence of elongated subgrains and grains perfectly aligned within regions resembling a former lamellar structure within bands supports the occurrence of such a mechanism.

Keywords: IF steel; Shear bands; Deformation twinning; Progressive subgrain misorientation recrystallization; EBSD

1. Introduction

Adiabatic shear bands (ASB) are regions where very large shearing occurs as a result of intense dynamic loading of metals and alloys. The amount of heat generated in this localized process is confined in the shear band and, for practical purposes, is not dissipated to the vicinity of the band. The term *adiabatic* refers to the short period of time where shear deformation occurs at a rate greater than the heat can be conducted away from the sheared zone. At high strain rates, ASB are a type of intense shear localization that depends on a number of metallurgical parameters, and their formation is often a precursor to catastrophic failures. In general, metals are frequently exposed to high strain rates and tend to display regions of highly localized straining when deformed plastically during conventional machining, metal-forming, impact, high velocity shaping or cryogenic behavior of materials to name but a few [1,2]. ASB in metals have been recently reviewed with respect to different engineering boundary conditions [3–5].

Many microstructural investigations have been performed to clarify both the flow localization and the shear evolution in copper [6–9], iron [9], refractory and hard metals [10–15], aluminum alloys [16–17], silicon carbide [18] and steels [19–23]. The scope of some of these studies consisted in determining the mechanical response of such materials under high rate loading and representing their flow stress behavior with the aid of constitutive mechanical models. There are many constitutive models describing the flow stress behavior of the materials in the literature, including those proposed by Johnson–Cook [24], Zerilli–Armstrong [25], Bodner–Partom [26] and Follansbe–Kocks [27] and all of these have been, to varying extents, applied to shear banding.

There have been many attempts to study the mechanisms of recrystallization in adiabatic shear bands. Hines and Vecchio [7]

* Corresponding author. Tel.: +55 24 3344 3012; fax: +55 24 3344 3029.
E-mail address: jfclins@metal.eeimvr.uff.br (J.F.C. Lins).

0921-5093/$ – see front matter © 2006 Elsevier B.V. All rights reserved.
doi:10.1016/j.msea.2006.12.019

have shown that the kinetics of two classical mechanisms for recrystallization, high-angle boundary migration and subgrain coalescence, as compared with the time–temperature profile determined for these adiabatic shear bands, are inadequate to explain the observed grain sizes, with the kinetics being several orders of magnitude slower than the deformation time and/or the cooling time of the shear bands. Tests conducted at liquid nitrogen temperature also demonstrated that temperature did not play a major role in dynamic recrystallization under these circumstances. Hines and Vecchio [7] proposed a dynamic recrystallization model, in which mechanically driven subgrain rotations assist the mechanism for recrystallization. This approach can enable dynamic recrystallization to proceed at very high strain rates, with only limited thermal assistance.

Later, Hines et al. [28] proposed a mechanical subgrain rotation model to account for the recrystallized grains, observed in adiabatic shear bands in a number of materials. The model is based on a 'bicrystal' approach using crystal plasticity theory to predict the evolution of subgrain misorientations by mechanical lattice rotations within ASB. These mechanically induced rotations are shown to occur at the high strain rate associated with adiabatic shear band formation. Recrystallized grain formation is proposed to occur by the formation and mechanical rotation of subgrains during deformation. Boundary refinement (recovery) is provided by the temperature rise and time necessary for dislocation rearrangement during deformation. This model is referred to as *Progressive subgrain misorientation* (PrisM) recrystallization and appears capable of accounting for shear band microstructures in a variety of metals.

TEM observations have been extensively employed to investigate the microstructure of ASB due to its tiny scale, which is in the range of a few nanometers. Nevertheless, the limited area illuminated in post-mortem TEM thinned disks provides poor statistical information. In order to enhance the statistical basis and determine the mesotexture and microtexture developed within shear regions, conventional and high-resolution EBSD techniques can be used to obtain accurate results. Humphreys reports in [29] that the use of FEG-SEM has improved the spatial resolution of EBSD allowing measurement of grains or subgrains as small as 0.1–0.2 μm in highly deformed materials. Only a few EBSD studies in ASB are reported in the literature. The first application of EBSD to shear band structure analysis was reported by Pérez-Prado et al. [15], which showed that significant misorientations occurred within the subdivisions of the shear band structure. In another recent investigation, regions in the vicinity of shear bands were successfully mapped, but not the structure within them [23]. In both of these works, only pole figures indicating large orientation spreads were shown. In addition, the microstructure developed within shear bands could not be resolved in detail. It is well known that the main problems in the conventional EBSD technique arise from inappropriate sample preparation and to the limited spatial/angular resolution in the SEM. These features have a strong influence on the indexing of the Kikuchi patterns. The Kikuchi patterns acquired from regions with high dislocation density are normally diffuse and cannot be indexed in a proper manner.

The final texture developed in IF steels is characterized by a sharp and homogeneous $\{1\,1\,1\}\langle u\,v\,w\rangle$ texture (γ-fiber) with components like $\{5\,5\,4\}\langle 2\,2\,5\rangle$, $\{5\,5\,4\}\langle 1\,3\,5\rangle$ and $\{1\,1\,1\}\langle 1\,1\,0\rangle$ [30–32]. The γ-fiber in bcc metals comprises orientations where $\{1\,1\,1\}$ planes are parallel to the normal direction (ND). At high rolling strains, shear bands become prominent in many metals and, depending on its volume fraction, can play an important role in determining the deformation texture. It is also well known that these deformation heterogeneities are favorable nucleation sites for further primary recrystallization. However, studies reporting jointly both the development of the deformation texture and the mechanical behavior in IF steels deformed at high strain rates are lacking in the literature.

In this work we report in detail the microstructure evolution within ASB induced in a hot-rolled IF steel deformed to large strains with aid of a split Hopkinson bar at −50 and 25 °C. The microstructural characterization of deformed specimens was performed using light optical microscopy (LOM), scanning electron microscopy (SEM), transmission electron microscopy (TEM) and electron backscatter diffraction (EBSD). High-resolution EBSD in a field emission gun scanning electron microscope (FEG-SEM-EBSD) was also employed to resolve the development of the new grain structure within shear bands.

2. Experimental

2.1. Material

The Ti-stabilized interstitial free (IF) steel used in this investigation was supplied by CSN (Brazil). The dimensions of the hot band were 250 mm in width, 300 mm in length and 38 mm in thickness. The plate was obtained by multiple-pass hot rolling in the austenite regime (1070 °C) followed by air-cooling. The chemical composition of the steel (in wt%) was the following: 0.003 C, 0.069 Ti, 0.003 V, 0.049 Al, 0.0025 N, 0.005 O, 0.19 Mn, 0.011 Si, 0.027 P and 0.005 S.

2.2. Dynamic compression and shear tests

Mechanical tests were performed at quasi-static ($0.001\,s^{-1}$) and dynamic strain rates (up to $3200\,s^{-1}$) at temperatures from −196 to 300 °C using cylindrical compression specimens of the IF steel, with the cylinder axis aligned parallel to the axis of the shear band samples. The results of these experiments were used to determine the coefficients and exponents of the Zerilli–Armstrong constitutive equation. This equation, in turn, was employed to estimate the temperature rise within the shear band region of the shear test samples.

The dynamic shear band tests were performed to shear strains (γ) in the range from 3.4 to 23.25, with test conducted at two temperatures, −50 and 25 °C. The dynamic tests were carried out in a modified split Hopkinson bar using hat-shaped specimens [33] (see Fig. 1). The specimens were carefully machined in the transverse section of the Ti-stabilized IF steel plate. AISI 4340 stopper rings were used to vary the shear strain (γ) in the material.

Fig. 1. Cross-section schematic drawing: (a) hat-shaped specimen used in this investigation (dimensions are given in mm) and (b) before dynamic compression test. SR refers to the stopper ring and the thickness of the ASB is given by ξ.

The shear strain in the shear localization was determined by the ratio between the displacement (δ) and the thickness of the shear band (ξ). The thickness (ξ) of each shear band was measured using LOM (dark field) in the central area of each specimen. It is well known that this method is not considered very rigorous because the thickness varies with distance but this region can be considered "homogeneous" to estimate the shear strain. In the upper and lower regions of the hat-shaped specimens the shear strains are generally higher than the central region due to its geometry that provides intense shear localization. The total displacement (δ) was calculated by the difference between of initial (h_1) and final (h_3) dimensions of the hat's height. Eight specimens divided in two sets were deformed at strain rates varying from 2.8×10^4 to $6.4 \times 10^4\ s^{-1}$ (Table 1). Table 1 also shows the nomenclature of the samples adopted in this work, the corresponding dimensions, the applied strain rates, and the thickness of the stopper rings used in the impact tests.

2.3. Microstructural characterization

Metallographic preparation for the EBSD measurements was carried out using a new methodology to reveal as many details of the microstructure as possible. Both polishing/etching operations performed in low carbon steels are usually based on electrolytic routes using hazardous $HClO_4$ containing solutions. In this work, we propose a simplified chemical–mechanical polishing route. A solution with 25 mL of a commercial colloidal silica suspension, 1975 mL of distilled water, 1 mL of nitric acid and 10 mL of commercial detergent was used as the polishing medium. The samples of shear region for TEM observation were obtained by sectioning in a low-speed diamond saw and electron discharge machine trepanning 3 mm disks. These disks were hand ground to 0.1 mm. A dimple grinder was used to thin the specimen mechanically to the thickness required for ion milling.

Light optical microscopy images were acquired in a Leica DM IRM microscope with conventional illumination (bright and dark fields). Electron channeling contrast maps of deformed specimens were obtained in a LEO 1450-VP scanning electron microscope operating at 10, 20 and 30 kV in the backscattered electron mode (BSE). This technique allows identifying regions with misorientations (ψ) around 2° or less by the variation in the gray scale in SEM images. Transmission electron microscopy was carried out in JEOL JEM-100CX operating at 100 kV.

2.4. Microtexture and mesotexture evaluation

The distribution of misorientations (ψ) across the grain boundaries and between pairs of adjacent grains or regions and the respective local texture developed within shear bands as well as at their edges was evaluated using the EBSD technique. Orientation imaging microscopy (OIM) results were determined by means of automatic indexing of Kikuchi patterns after suitable image processing in a TSL EBSD system interfaced to a Philips XL-30 SEM operating at 30 kV with a W-hairpin filament. The more detailed mapping of representative specimens was conducted in a JEOL JSM-6500F field emission scanning electron microscope (FEG-SEM) operating at 15 kV also interfaced to a TSL EBSD system.

Table 1
Nomenclature, strain rates and dimensions of the hat-shaped specimens deformed in a split Hopkinson bar following the dimensions in Fig. 1a

Sample	h_0 (mm)	d_0 (mm)	h_1 (mm)	d_1 (mm)	h_2 (mm)	d_2 (mm)	h_3 (mm)	SR (mm)	Temperature (°C)	Time (μs)	Strain rate ($10^4\ s^{-1}$)
A-1	8.10	18.92	6.71	10.01	6.83	9.45	6.22			51	2.80
A-2	7.98	19.00	7.01	10.16	7.16	9.70	6.35	6.50	25		
A-3	8.05	19.02	6.88	10.11	7.06	9.60	6.50	25	5.23		
A-4	7.80	19.02	7.06	10.13	6.96	9.73	6.22	6.50	−50	33	6.24
B-1	8.13	19.10	6.71	10.13	6.22	9.70	4.95			122	6.24
B-2	8.03	19.05	6.99	10.16	7.11	9.68	5.00	5.00	25		
B-3	7.85	19.05	7.04	10.16	7.01	9.68	4.98	122	6.38		
B-4	8.13	19.05	6.88	10.16	7.26	9.68	4.95	5.00	−50	122	5.59

SR refers to the thickness of the stopper ring and h_3 is the final height of the hat-shaped specimen after dynamic shear deformation.

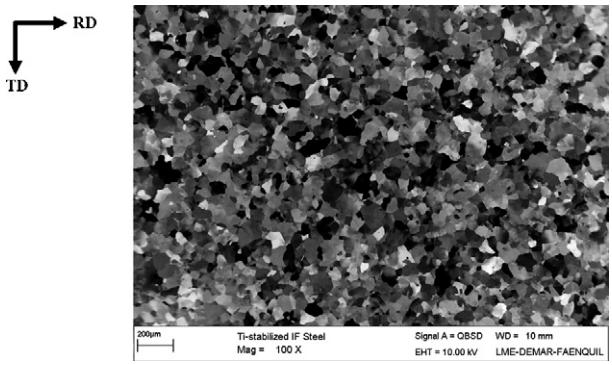

Fig. 2. Electron channeling contrast image of longitudinal section (rolling plane) of the initial Ti-stabilized IF steel plate. RD and TD refer, respectively, the rolling and transversal direction.

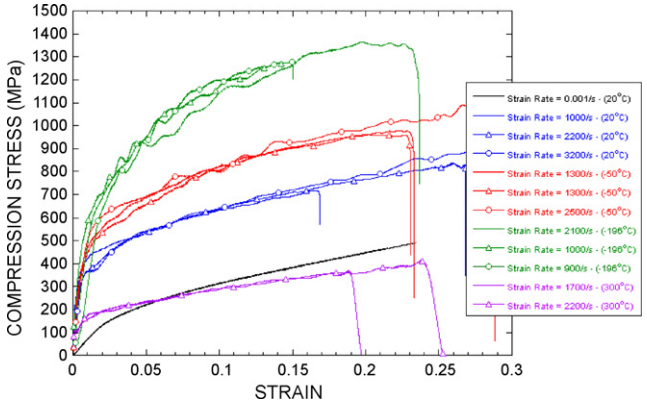

Fig. 3. Stress–strain response at several temperatures for strain rates varying from 0.001 to 3200 s^{-1} for IF steel.

3. Results and discussion

3.1. Starting material

The starting material was evaluated in terms of its microstructure and texture. Results showed the existence of a very weak and diffuse (random) texture in the hot-rolled plate resulting from the transformation of austenite into ferrite polygonal structure after air-cooling. The microstructure of the IF steel plate consists of a ferritic matrix and Ti-rich particles. The average orientation density (OD) found in the hot-rolled plate was about 3.42. Hardness results showed a mean value of 98 ± 13 Vickers. In the rolling plane, hardness was about 109 ± 6 Vickers whereas this value dropped to about 86 ± 4 Vickers in the transverse section, i.e. the plane containing both the rolling (RD) and the normal directions. A comparison between the linear intercept method by EBSD technique and a traditional quantitative metallography determination using LOM was performed to estimate the grain size. Good agreement was observed when comparing the results obtained from both techniques. According to both methods the grain size was equal to 55 ± 6 μm. Fig. 2 shows a micrograph of the rolling plane (RD–ND section).

3.2. Deformed state

Fig. 3 shows the stress–strain response of IF steel at strain rates ranging from 0.001 to 3200 s^{-1} at temperatures varying from −196 to 300 °C. It is well known that body-centered cubic (bcc) metals display strong temperature sensitivity to their stress–strain response. The stress–strain curves in Fig. 3 display considerable strain rate sensitivity driven by strong Peierls–Nabarro stresses, and its associated strong thermal activation energy dependence. Pérez-Prado et al. reported similar behavior in dynamically compressed tantalum and Ta–10 wt% W alloy at strain rates varying from 0.001 to 10,000 s^{-1} at temperatures from 25 to 525 °C [15]. These results showed Ta–10 wt% W alloy was less sensitive to the thermal softening displayed by pure tantalum strained in the same conditions.

The width of the shear band (ξ) within the samples was determined using LOM and confirmed by SEM. The results are shown in Table 2 along with the calculated values of the shear (γ) and longitudinal (ε) strain components. The conversion from shear strain to longitudinal strain (ε) has been calculated with the aid of the following equation:

$$\varepsilon = \ln\left(\frac{\gamma^2}{2} + \gamma + 1\right)^{1/2} \quad (1)$$

There is a clear fluctuation of the shear strain found between both sets of the dynamically deformed specimens at 25 °C and the stopper ring thickness, as well as the corresponding shear band widths. At lower testing temperatures, this fluctuation was less evident, and therefore only one sample from each set at this condition was used for the more complete analysis reported herein. It was observed, as a general trend, that the shear strain value increases with the decrease of the stopper ring's thickness and the test temperature.

Fig. 4 shows a general view of the deformed shear region in different test conditions. The irregular shape of the shear bands and their respective macroscopic displacement (δ) in the shear regions are revealed in these micrographs. Therefore, it is well known that the shear strain varies along the thickness of the shear band. Chen et al. [12] pointed out the problems that arise when the thickness of the shear band ξ, is determined as indicated in Fig. 1b.

Deformation twins are found extensively throughout the shear deformation regions in both groups of the investigated samples, as shown in Fig. 5. Twinning in bcc metals is very

Table 2
Deformation parameters for the dynamic shear tests (δ is the displacement, ξ is the thickness of the shear band, γ is the shear strain and ε is the true strain)

Sample	Temperature (°C)	δ (mm)	ξ (μm)	$\gamma = (\delta/\xi)$	ε
A-1		0.48	133.4	3.62	1.21
A-2	25	0.66	169.9	3.89	1.26
A-3		0.38	112.0	3.40	1.16
A-4	−50	0.71	121.8	5.84	1.59
B-1		1.75	218.9	8.01	1.86
B-2	25	1.98	161.6	12.26	2.24
B-3		2.06	126.3	16.29	2.51
B-4	−50	1.88	80.9	23.25	2.85

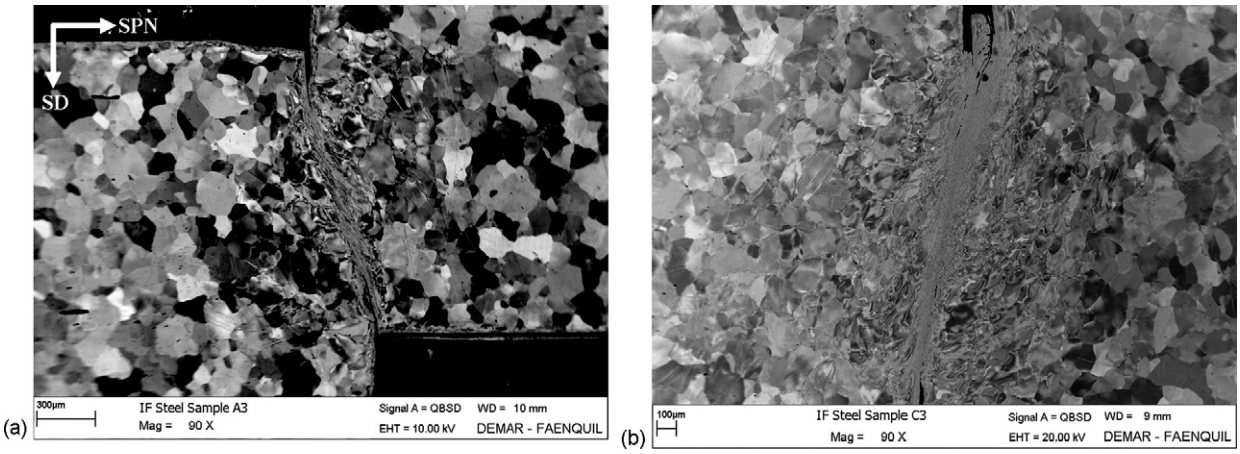

Fig. 4. General view of the shear region in samples: (a) A-3 and (b) B-3. The shear direction (SD) in the micrograph is the vertical one. SPN stands for shear normal plane (SEM-BSE).

sensitive to temperature and strain rate conditions, and our deformation conditions associated with the dynamic loading at low temperatures (25 and −50 °C) facilitates the occurrence of deformation twinning as an alternative deformation mode to dislocation slip. The size and morphology of the deformation twins vary from one region to another within the same specimen. These twins are bounded by incoherent interfaces and exhibit a lenticular shape independent of the test temperature. A slight increase in volume fraction of deformation twins was noted in specimens deformed in cryogenic conditions. It was also observed that deformation twins become thinner with decreasing test temperature; however the volume fraction of twins was not quantitatively determined in the present investigation. Mechanical twinning gains importance because of the

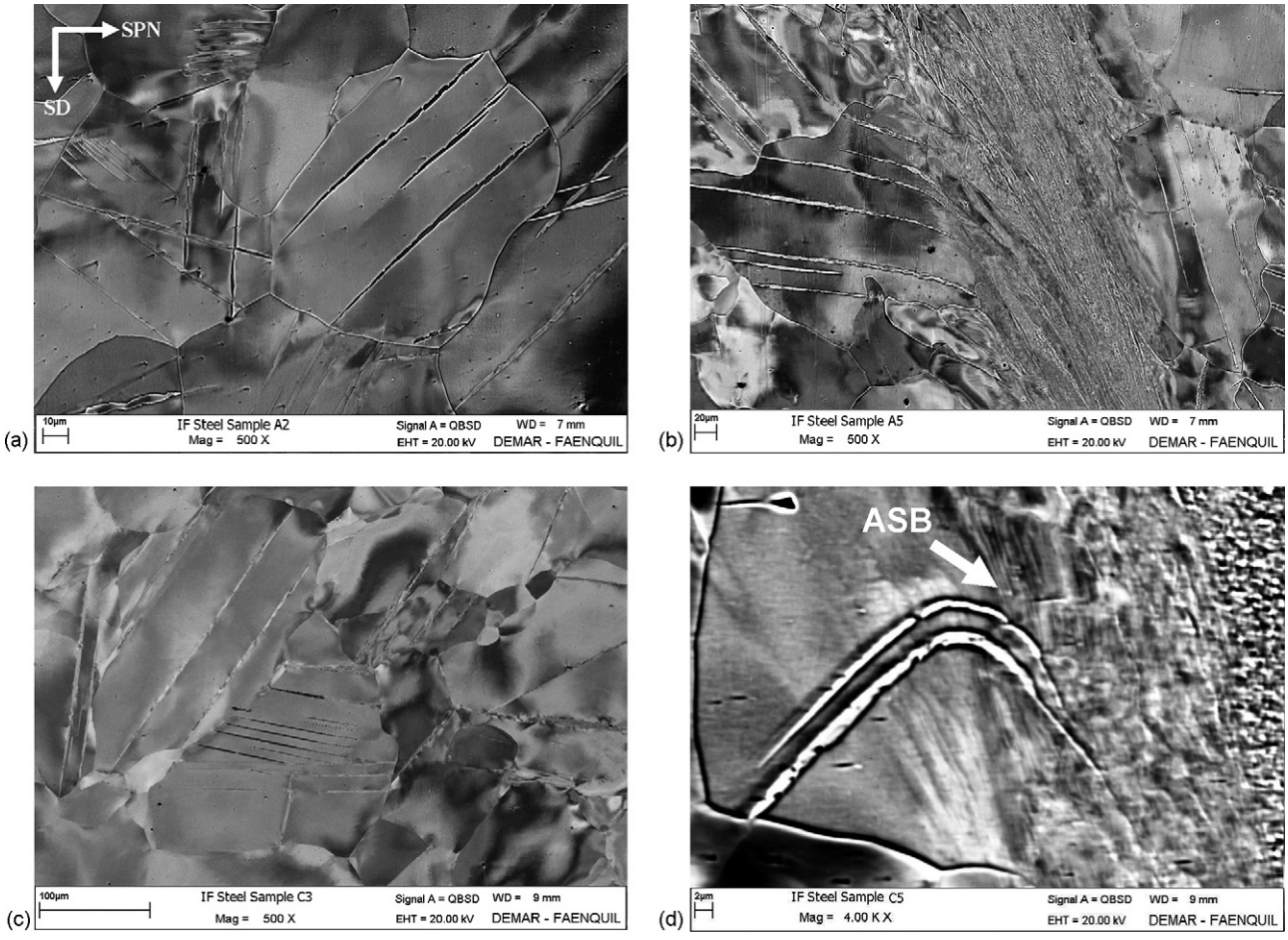

Fig. 5. Micrographs showing deformation twins in samples: (a) A-2, (b) A-4, (c) B-3 and (d) B-4. The shear direction (SD) in the micrograph is the vertical one. SPN stands for shear plane normal (SEM-BSE, 20 kV).

strengthening provided by the increasing number of barriers for dislocation motion in metals. The literature reports that twinning in bcc metals is preferentially associated with {1 1 2} planes rather than with {1 1 0} [34]. Deformation twinning is also grain size dependent in high strain rate processes. As a general trend, the twinned volume fraction increased with increasing strain. The literature also reports the presence of deformation twins at different temperatures and strain rates in pure iron (single and polycrystals) and extra-low-carbon steel without microalloying elements [17,21,35–38]. Bowed twins in grains close to the adiabatic shear bands (marked by white arrow in Fig. 5d) were observed in all of the specimens. This peculiar morphology strongly suggests that deformation twinning occurs before the flow associated to shear band over the microstructure. Meyers et al. [39] reported similar findings in α-Ti after shear deformation.

Figs. 6 and 7 display the micrographs taken within the adiabatic shear bands. Voids, blunt cracks and others damage induced by high strain rate deformation processes are also seen in the shear region (Fig. 6c). A similar behavior was observed in adiabatic shear bands in the AISI 4340 steel deformed at $0.8 \times 10^6\ s^{-1}$ with accumulate shear deformation about 3.92 [20]. The literature reports that the morphology of the voids can be associated with the ductility of the material at high strains. Grebe et al. [10] reported the voids observed in Ti–6Al–4V as having a spherical morphology after impact ballistics experiments. Similar findings were observed in our IF steel specimens in the shear deformation zone.

Many authors report that the microstructural characterization of shear bands using LOM and SEM techniques is unfeasible due to resolution limitations [16]. As expected, it is not easy to resolve details of the microstructure found in the fine lamellar structure developed during plastic deformation using a conventional W-filament SEM in the BSE mode. The lamellae spacing found in the shear bands is mostly below 0.5 μm. For this reason, TEM is typically the most suitable technique to resolve details of this lamellar structure. Fig. 7 shows the lamellar structure (samples A-1 and A-4) and a well-defined elongated subgrain structure within the ASB (sample A-4). It is worth mentioning that the recrystallization models that describe the microstructural evolution within ASB include a step that involves the formation of elongated subgrains by recovery processes.

The data in the plots of stress–strain curves (Fig. 3) was used to estimate the temperature rise during adiabatic dynamic compression tests of this IF steel incorporating the work of plastic deformation. The temperature rise certainly plays an important role in the recovery processes during straining and further cooling down to room temperature. There is no direct experimental technique to measure this increase in temperature due to the

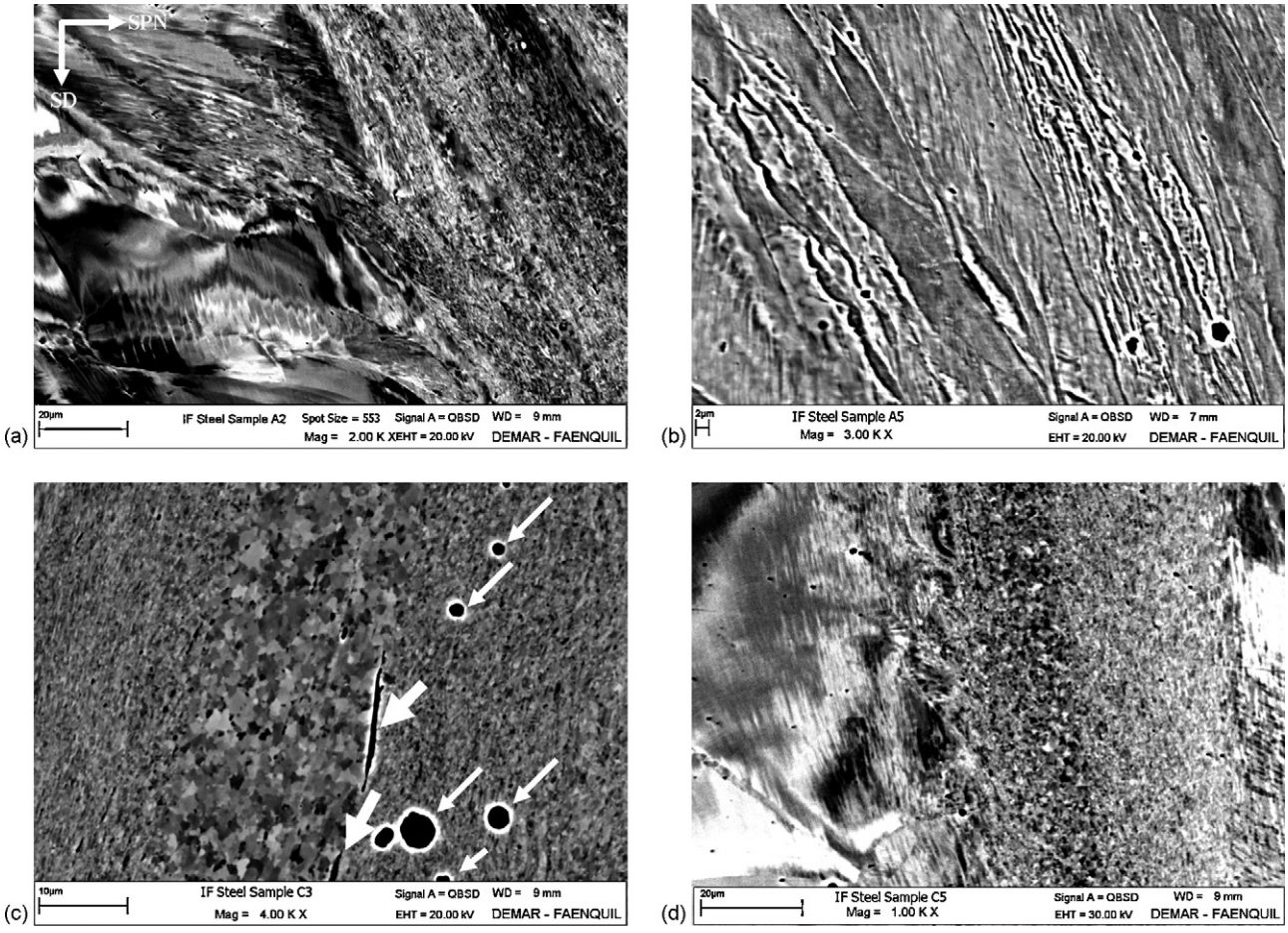

Fig. 6. Micrographs showing details of the microstructure of ASB in samples: (a) A-2, (b) A-5, (c) B-3 and (d) B-4. The shear direction (SD) in the micrograph is the vertical one. SPN stand for the shear plane normal (SEM-BSE).

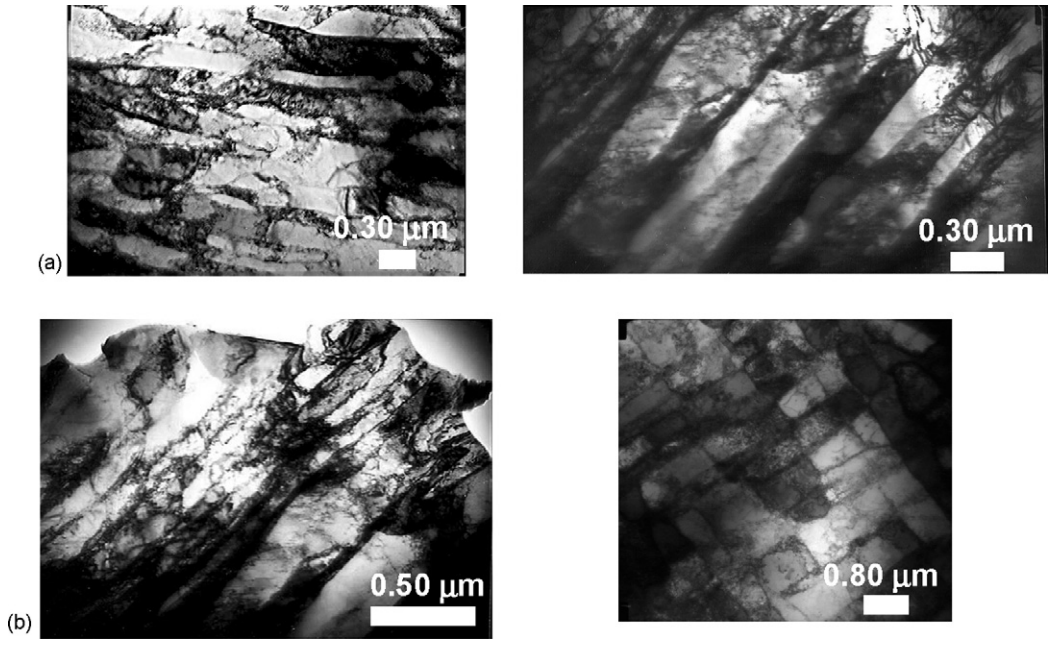

Fig. 7. Micrographs showing details of the microstructure of ASB in samples: (a) A-1 (lamellar structure), (b) A-4 (lamellar structure and elongated subgrains) (TEM, bright field, 100 kV).

short duration of the compression tests and boundary conditions. The determination of the coefficients and exponents of the Zerilli–Armstrong constitutive equation was done by regression analysis technique that determines the best-fit parameters for all of the data. Eq. (2) gives the constitutive equation used for this analysis:

$$\sigma = \sigma_o + C_1 \exp[-C_2 T + C_3 T \ln(\dot{\varepsilon})] + C_4 \varepsilon^n \quad (2)$$

where σ_o, C_1, C_2, C_3, C_4 and n are the parameters determined by regression analysis procedure, $\dot{\varepsilon}$ is the true imposed strain rate, T is the temperature and σ and ε (Table 2) are the stress and strain, respectively. It is worth mentioning that due to uncertainties associated with shear area and shear displacements within hat-shaped specimens, the temperature rise was calculated by integrating the Zerilli–Armstrong constitutive equation using the shear band deformation conditions, and assuming a portion of the work is converted to heat, represents an estimate of the actual shear band temperature. In problems of high strain rate deformation, it can be assumed that typically ~90% of plastic work done during dynamic deformation produces heat [5]. Thus, the ASB temperature rise can be estimated using the expression:

$$T = \frac{0.9}{\rho C_p} \int_0^{\varepsilon_f} \sigma \, d\varepsilon \quad (3)$$

where ρ is the material's density, C_p the heat capacity and σ is given by the Zerilli–Armstrong constitutive equation (Eq. (2)) integrated from 0 to the final strain (ε_f). The results of this calculation are depicted in Fig. 8. This final strain is obtained by converting shear strain in the shear band to axial strain via Eq. (1). Fig. 8 shows clearly that when the shear strains are greater than 5.84 (sample A-4) the estimated temperature rise can attain about 1000 °C. In theory, this instantaneous amount of heat coupled with the elevated local dislocation density could run away both recrystallization and/or recovery process during the deformation process of the IF steel. At low strain rates it is well-documented that dynamic recrystallization is a common feature during the hot-rolling stage (~1070 °C) of ultralow-carbon steels [40]. In addition, the average time duration (~77 μs) of the tests and consequently the temperature rise in adiabatic conditions is reported in the literature as generally lower than the minimum time required to associate with static recrystallization process [41].

In contrast to the fine lamellar structure found in most of the samples, a striking feature observed in some deformed specimens is the presence of an equiaxed grain structure strip within shear bands (Fig. 6c and d). This structure probably results from some sort of dynamic recrystallization process in particular areas within the shear bands, and what mechanism is still controversial

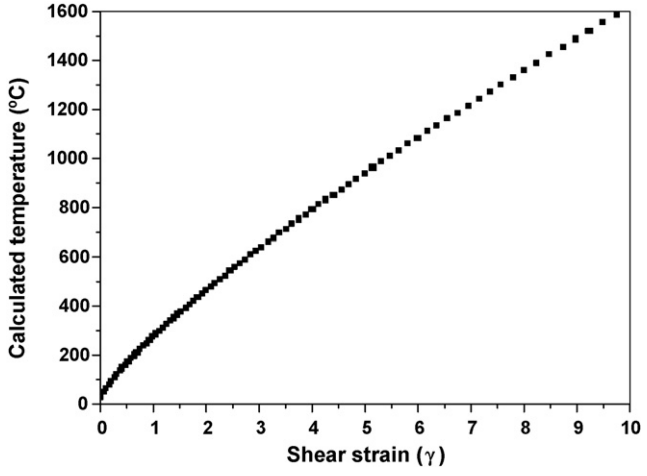

Fig. 8. Calculated temperature rise for IF steel as function of shear strain using the Zerilli–Armstrong equation.

at this time. Several studies reported the occurrence of recrystallization under high strain rate conditions in various materials [7,15,23]. The mechanism known as rotational dynamic recrystallization, formerly proposed by Derby [42] and later modified by Meyers et al. in [16], is a likely mechanism to explain this new grain structure within ASB incorporating the dislocation energetics in the model. The microstructural evolution involved in this mechanism can be summarized as follows: (i) rearrangement of dislocations into elongated cells with increasing strain; (ii) the thermal activation provided by the temperature rise and the development of increasing misorientations transform these cells into elongated subgrains bounded by many high-angle lamellar boundaries; (iii) subdivision of these elongated structures with the creation of geometrically necessary boundaries associated to local crystal rotations [16]. These aspects are captured numerically in the work of Hines et al. [28].

Hines et al. [28] proposed a mechanical subgrain rotation model to account for the recrystallized grains within ASB in a number of materials. The model is based on a 'bicrystal' approach using crystal plasticity theory to predict the evolution of subgrain misorientations. These mechanically induced rotations were shown to occur under the high strain rate associated with adiabatic shear band formation. Recrystallized grain formation was proposed to occur by the formation and mechanical rotation of subgrains during deformation, coupled with boundary refinement via diffusion during shear band cooling. After the deformation process, the boundary refinement occurs by reducing the excess dislocation dipoles promoted mainly by dislocation climb during the cooldown stage. This model is referred to as *progressive subgrain misorientation* (PriSM) recrystallization and appears to account for shear band microstructures in a variety of metals. Hines and Vecchio [7,28] have shown by careful thermal diffusion calculations of dislocation structures in shear bands that there is insufficient time during the deformation period of shear band formation to achieve any significant dislocation annihilation and boundary refinement. However, since the shear band temperature rise is fairly high and the cooling period of the shear band is significantly longer than the deformation time, it is quite reasonable, kinetically speaking, to achieve significant dislocation annihilation and boundary refinement during the cooling period of the shear band. The only significant differences between these various mechanisms related to whether one believes that the formation of the equiaxed structure with refined high-angle boundaries occurs entirely during the deformation time (dynamic recrystallization [28]) or whether the misorientation portion of the recrystallized structure occurs during the deformation time and the majority of the dislocation recovery and boundary refinement occurs during the cooling period [29].

3.3. Deformation microtexture

Conventional EBSD has proved being a suitable technique to investigate the grain subdivision behavior displayed by grains in the vicinities of the shear bands. However, due to the large stored energy in the lamellar structure found within ASB, most of Kikuchi patterns obtained using conventional SEM-EBSD are diffuse. As a consequence, the corresponding orientation data points must be discarded because they cannot be properly indexed. This is an intrinsic limitation of the spatial resolution of the conventional technique (W-filament). In contrast, the use of high-resolution EBSD has proved to be a powerful tool to bring out details of the microstructure and the resulting misorientations present in the lamellar structure. In the literature regarding microstructural characterization of isothermal shear bands, there are only a few results reported using FEG-SEM-EBSD in [43] for a low-strained Al–Mg alloy deformed in plane strain compression. In high strain, high strain rate deformation the observations within ASB are recent and previously limited to conventional EBSD mappings, with the very first reported use of EBSD on shear bands to be Pérez-Prado et al. [15] on tantalum, and more recently by Meyers et al. [23].

3.3.1. Group A

The EBSD characterization was performed on specimens of Group A. Fig. 9 shows the results of the EBSD mapping in sample A-3 ($\gamma = 3.4$). The OIM map was performed in five areas with a step size of 0.1 μm. The average width of the shear band in this orientation map is about 112 μm. This figure shows details of the lattice rotations within the shear band and long-range internal stresses associated to grain subdivision in the vicinity of the shear localization. The sharp Kikuchi patterns could be obtained within a shear band and the respective pole figures have shown a gradual lattice rotation around α-fiber to accommodate the severe plastic deformation imposed. This lattice rotation can be observed in terms of the reorientation around the shear plane normal direction (SPN) in relation to the ideal orientation ⟨1 1 0⟩//SD (α-fiber). SD stands for shear direction. It is worth to mentioning that the morphology of this shear band is very irregular in contrast with other samples deformed to larger strains (Group B). Take note of a nearly $[\bar{4}\,\bar{1}\,3]$-oriented deformation twin bending towards the shear localization within an $[2\,\bar{1}\,0]$-oriented grain. It represents a simple example of the many twins found throughout the microstructure. The literature reports that several twinning systems can operate under compressive loading and exhibit a complex orientation-dependency [44,45]. It can be concluded that the shear band displays a strong heterogeneous character in terms of the grain fragmentation and for this level of shear strain only recovery mechanisms could be observed. There is so sign of recrystallized grains within the ASB.

In copper, dynamic recrystallization was observed to occur at a certain value of shear strain ($\gamma \approx 4$, at a strain rate of $4.10^4\ s^{-1}$) [7]. However, Ta and Ta–10W alloys do not exhibit a new recrystallized structure within regions of highly localized deformation in the hat-shaped specimens deformed to an equivalent shear strain [15]. As mentioned before, one would expect that recrystallization become noticeable at a shear strain of approximately 5.85 (sample A-4) in IF steel due to the significant temperature rise. Two EBSD mappings were performed to investigate the possible presence of recrystallized grains within the shear region of sample A-4. Contrasting to sample A-3, the ASB found in sample A-4 (Fig. 10a) displays a more uniform morphology and was mapped with a step size of 0.1 μm. It can be observed that some degree of subdivision (long-range stresses) within the adjacent grains and the presence of slip bands and

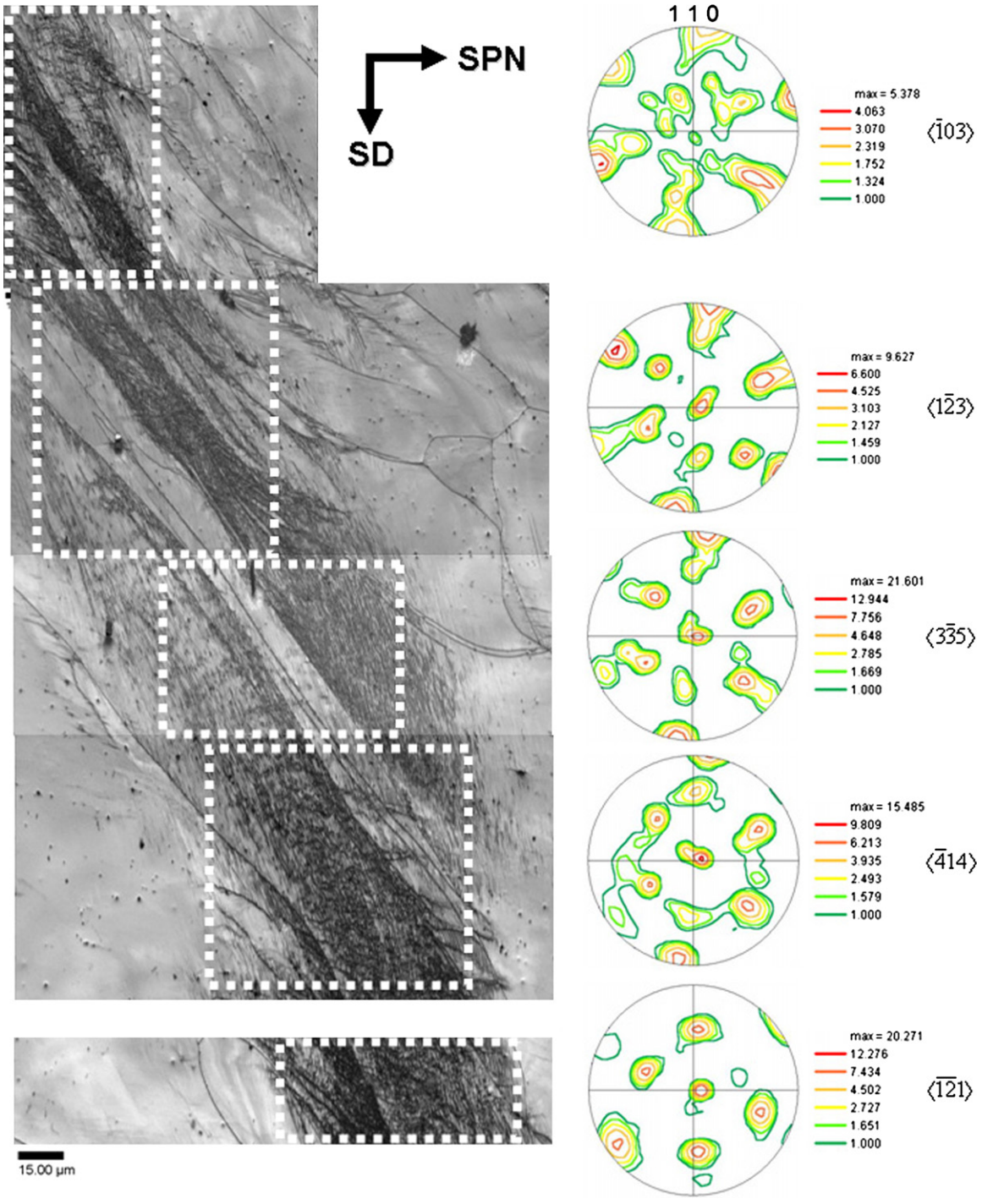

Fig. 9. High-resolution EBSD results of sample A-3 showing image quality (IQ) map version of the OIM (not shown in this paper) and {1 1 0} pole figures of each area marked (white rectangle) in IQ map, respectively.

deformation twins. The literature reports that these bands appear within grains and exhibit a well-defined crystallographic direction [44,45] and deformation twins are reported quite often [34]. It is important to note that under large strain rates, these slip bands were also found. Fig. 10a shows the microstructure of the ASB in sample A-4 consisting on fine lamellar boundaries, elongated subgrains and many ultrafine recrystallized grains. As mentioned before the TEM micrographs also showed the same lamellar boundaries and elongated subgrains. These ultrafine-grained structures could be clearly distinguished in the deformed microstructure in the quality image maps from EBSD. The second OIM map (Fig. 10b) shows that the new grain structure has a mean size of about 0.3 μm. These results strongly suggest that these new grains have their origin closely related to former lamellar structure. The analysis of microtexture within ASB (Fig. 10c) indicates a weak component near [1 $\bar{2}$ 2]. In this orientation map, the fraction of boundaries with misorientations comprised in the interval $15^\circ \leq \psi < 180^\circ$ was found to

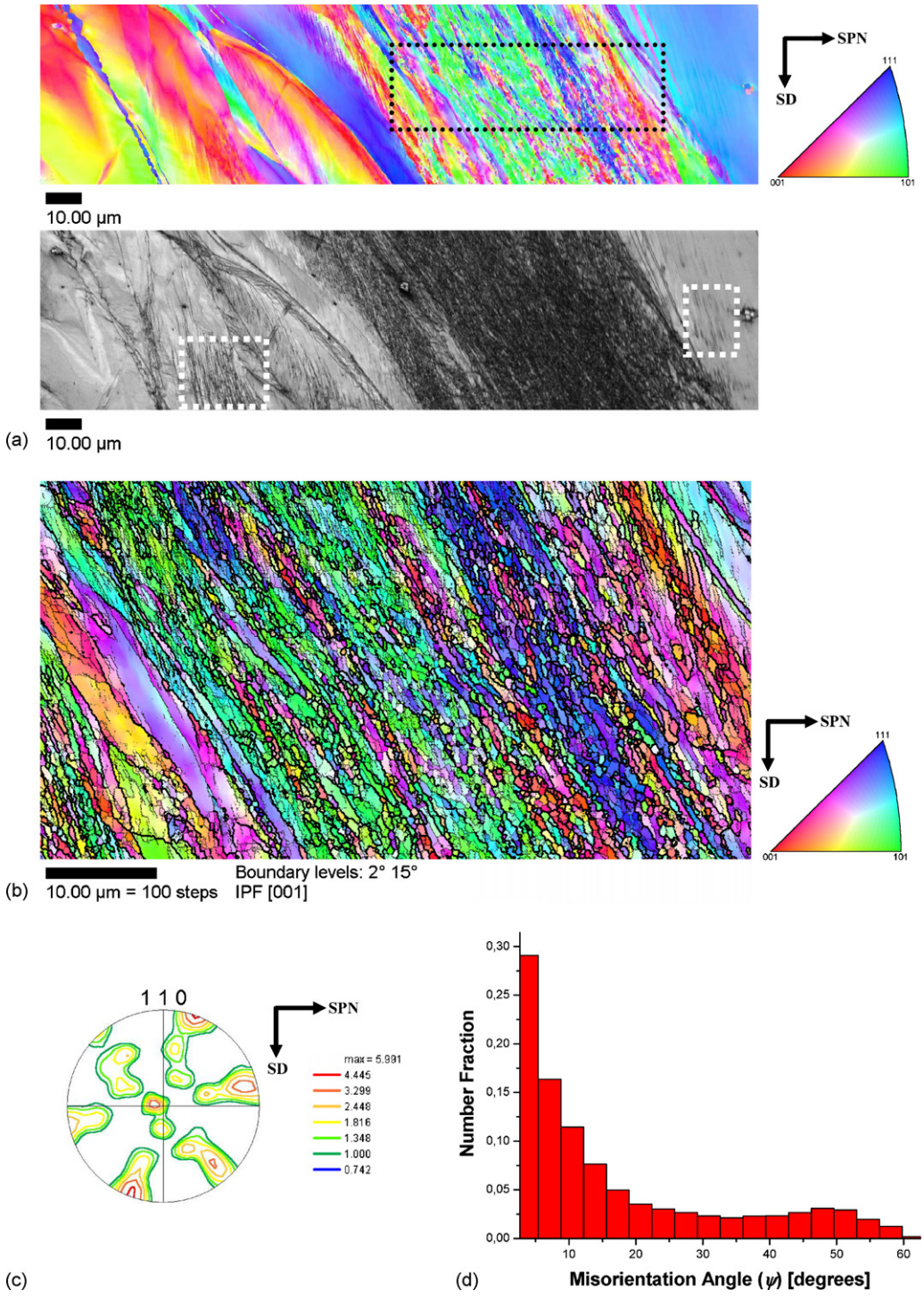

Fig. 10. OIM results of the shear region of the sample A-4: (a) OIM and image quality map, (b) orientation map of ASB indicated in (a) showing high (thick black line) and low angle character (fine black line) of boundaries, (c) {1 1 0} pole figure corresponding to the mapped area showed in (b) and (d) boundaries distribution displayed in (b). The shear direction (SD) in the micrograph is the vertical one. SPN stand for the shear plane normal. Note that the areas marked within white rectangles indicate slip bands in (b).

be lower than 35% (Fig. 10d). Due to the high fraction of low angle boundaries and the presence of elongated subgrains, it is plausible considering sample A-4 underwent dynamic recovery supported by lamellar boundaries refinement with the development of a small fraction of new ultrafine grains. Furthermore, the presence of a clear texture (around the α-fiber) within the ASB indicates that the new grains do not result from a nucleation and growth or from a diffusion-controlled recrystallization process (neither static recrystallization by nucleation and growth or subgrain coalescence). In contrast, the presence of the consistent fiber texture supports the idea of the new grains evolving from the plasticity of the shear region, and is therefore consistent with

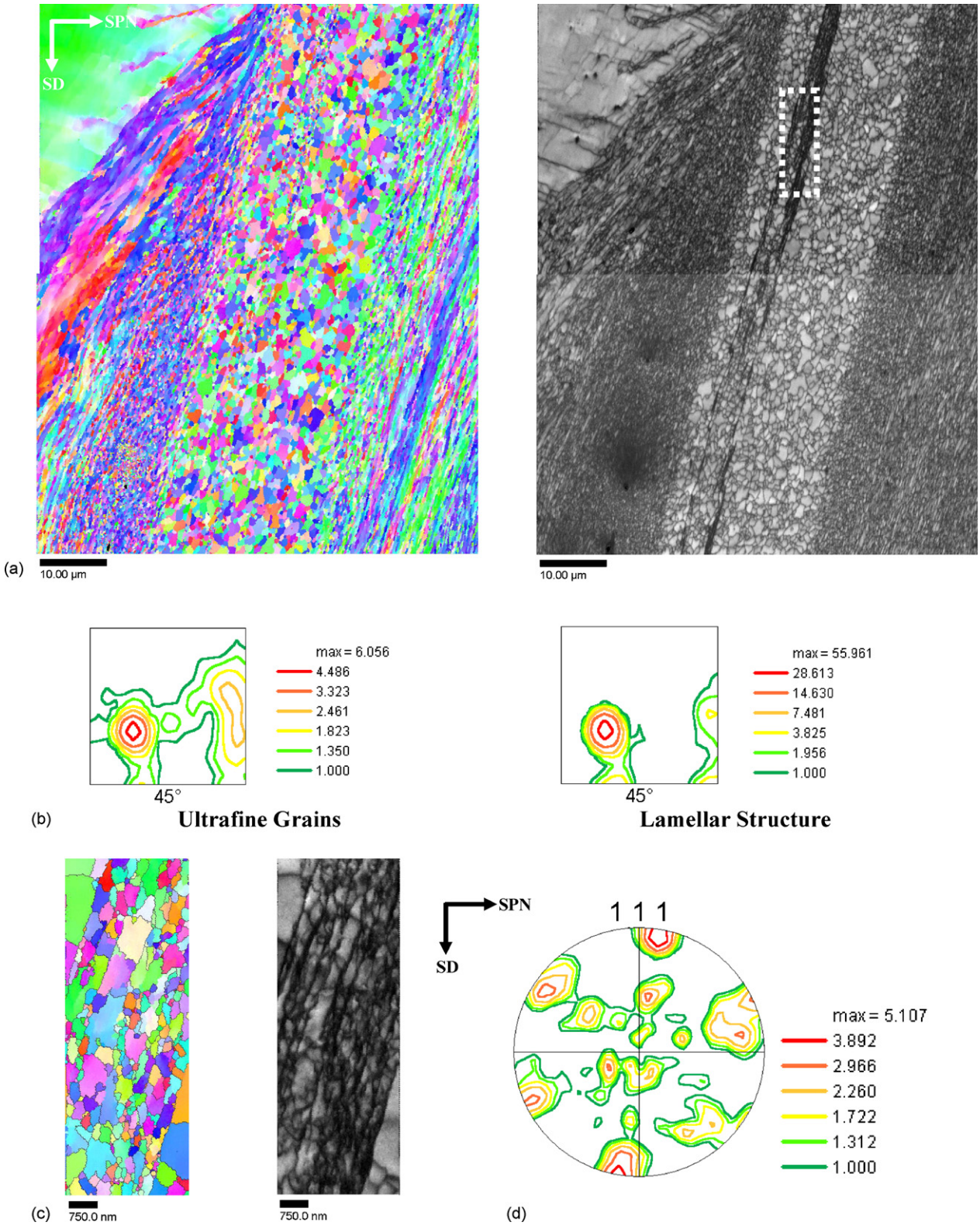

Fig. 11. OIM results of the shear band of the sample B-3: (a) OIM and image quality map, (b) ODF showing $\varphi 2 = 45^\circ$ corresponding to ultrafine grains and lamellar structure, (c) enlarged view of the region marked in (a) (white dashed rectangle) and (d) {1 1 1} pole figure corresponding to region scanned in (c). The shear direction (SD) in the micrograph is the vertical one. SPN stand for the shear plane normal.

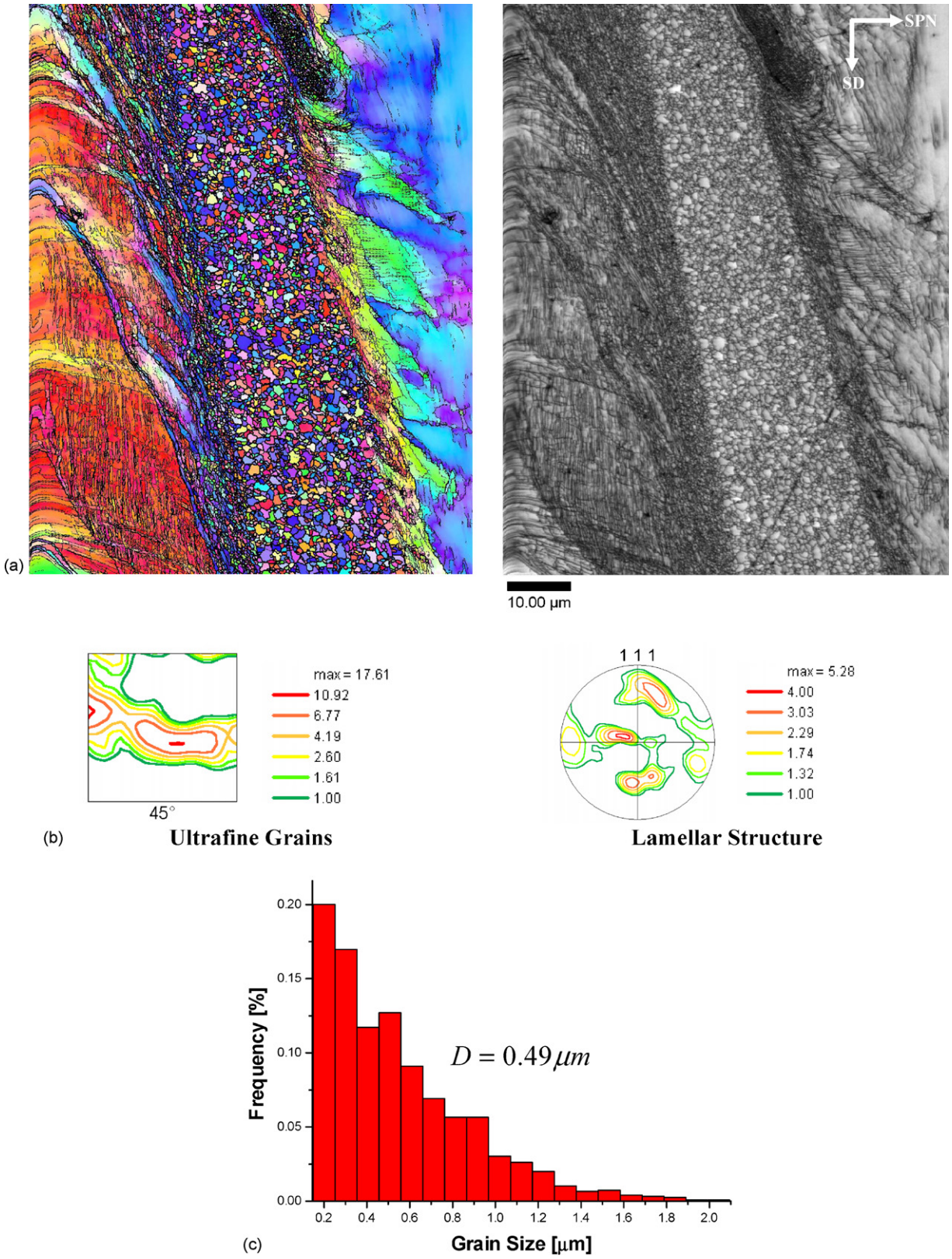

Fig. 12. OIM results of the shear band of the sample B-4: (a) OIM and image quality map, (b) microtexture corresponding to ultrafine grains and lamellar structure in (a) and (c) grain size distribution of the new grain structure displayed in (a).

the dynamic shear deformation leading to subgrain development and their rotation, simultaneous with (dynamic) or followed by (static) boundary refinement associated with recovery processes; the latter being consistent with the *progressive subgrain misorientation* mechanism proposed by Hines et al. [28] and the recovery kinetics calculations of Hines and Vecchio [7].

3.3.2. Group B

SEM shows the presence of a fine-grained structure in the central region of the ASB (sample B-3) in Fig. 6c. These new equiaxed grains are surrounded by a well-developed lamellar structure, typically found in metals deformed to large strains. The width of the ASB displaying the recrystallized structure is about 30 μm. A small step size (0.1 μm) was used to perform this orientation mapping (Fig. 11a). Results show the presence of regions with low density of defects (grains) within the lamellar structure as can be clearly identified by the image quality (IQ) map. The average misorientation across these lamellar dislocation boundaries is about 55° (high-angle character). The lamellae spacing found in the shear band is about 0.2–0.3 μm. The orientation distribution function (ODF) of the recrystallized grains within the ASB indicates a clear and strong γ-fiber texture and a weak α-fiber (Fig. 11b). The mean grain size in this recrystallized structure is about 0.45 μm. The striking aspect in these findings is the similarity between the texture displayed by recrystallized grains within the ASB and the recrystallization texture frequently reported in IF steels processed by cold rolling followed by isothermal annealing [30].

The white dashed rectangle marked in Fig. 11a shows the presence of an interesting region within ASB. It is possible to observe very tiny strips in the left part of a well-defined recrystallized band (below 1 μm in thickness). The microstructure within these tiny strips differs from the surrounding recrystallized areas. An interesting microstructure consisting of a few lamellae containing elongated subgrains can be seen within these strips (Fig. 11c). Note the large fraction of high-angle boundaries in the substructure marked by black lines. The microtexture corresponding to this strip, in particular, also belongs to a weak γ-fiber (Fig. 11d). It is worth mentioning that only a few crystallites were taken into account to determine the {1 1 1} pole figure. Nevertheless, the presence of a weak microtexture and lamellar boundaries associated with the elongated subgrains found in this region strongly suggests the occurrence of dynamic recovery as discussed in the samples of Group A, in particular, sample A-4.

In order to resolve details of the microstructure, sample B-4 was also mapped via field emission microscope interfaced with EBSD system. This specimen was chosen because of the presence of a clear grain structure within a shear band resolved by SEM (see Fig. 6d). Fig. 12a shows the orientation map performed in the shear region and reveals details of the microstructure where recrystallized grains with equiaxed morphology are seen embedded in the fine lamellar structure of the shear band. The recrystallized grains are confined within a 30 μm wide region making about 26° with SD. This orientation map was performed in area of 70 μm × 90 μm with a step size of 0.1 μm. The fine and thick black lines in the OIM mark, respectively, low and high-angle boundaries. In the vicinity of the sheared region (red grain), we note the presence of a well-defined (left part) subgrain structure. The mean subgrain size in this 56°[1 0 0]-oriented grain is about 1 μm. Deformation twins bending towards the shear direction are noticeable in the left part of the OIM. In the right part of the OIM, one can notice this region display a stable pattern in terms of grain subdivision. The literature reports that this behavior could be described in terms of active slip systems of grains oriented near {0 1 1}⟨1 1 1⟩//SD that do not undergone several rotations under severe shear deformation. The {0 1 1}⟨1 1 1⟩-slip system have the highest resolved shear stress for bcc metals.

Based on the ODF shown in Fig. 12b the orientation of the ultrafine grains belongs to the γ-fiber. In contrast with the results observed in sample B-3, the lamellar structure is weakly oriented to the γ-fiber as shown in the {1 1 1} pole figure. The literature reports that the final and stable orientation for ASB is around ⟨1 1 1⟩. This result could also indicate an intense restoration process within the lamellae (dynamic recovery) lowering the intensity of the γ-fiber. It is worth mentioning that we have cropped a region within the ASB containing only recrystallized grains and only these grains were accounted for the determination of the mean grain size and corresponding local textures. It can be concluded that the new recrystallized grains (about 5000 grains) have a mean grain size of about 0.49 μm (Fig. 12c).

For the first time, the microstructure, in terms of both apparent grain size and grain orientation (or texture) of an induced shear band has been revealed in a statistical basis due to high spatial resolution of the FEG-EBSD technique. The results presented in this paper support *progressive subgrain misorientation* recrystallization [28] coupled with grain boundary refinement via recovery processes during the dynamic shear band formation in the IF steel. This mechanism could satisfactorily explain the development of the new ultrafine grain structure within the ASB. Many authors report evidence supporting this mechanism based on a quite limited statistical basis provided by TEM observations. The effect of temperature rise, strain rate and large strains imposed could explain the differences of the volume fraction of the recrystallized grains and the differences in texture observed in the two sets of sample examined here.

4. Conclusions

Hat-shaped specimens of a hot-rolled IF steel were dynamically compressed in a split Hopkinson bar at high strain rates to induce the formation of adiabatic shear bands. Deformation twins were found throughout the microstructure, in particular close to the shear bands. The volume fraction of twinned grains was larger in the samples deformed at cryogenic conditions (50 °C). The presence of deformation twins bending towards the shear direction strongly suggests that mechanical twinning occurs before the flow associated to shear banding. FEG-SEM-EBSD results show that most grains adjacent to the shear bands subdivide into a well-defined subgrain structure. An interesting feature observed in many specimens, independent of test temperature, was the presence of an equiaxed grain structure with distinct textures: a weak and sharp α-fiber (Group A) and γ-fiber (Group B) within the ASB. Furthermore, the presence of

elongated subgrains and grains aligned with the shear direction in the former lamellar structure within the ASB also supports the occurrence of *Progressive subgrain misorientation* (PrisM) recrystallization to explain the development of the ultrafine-grained structure.

Acknowledgements

The authors are indebted to FAPESP for the financial support (Grant Number 01/14543-9), to CAPES-DAAD, to CNPq (Brazil) and to Mrs. Katja Angenendt and Dipl.-Ing. Alice Bastos da Silva (Max-Planck-Institut für Eisenforschung GmbH, Germany) for their kind assistance in the FEG-SEM-EBSD measurements. Thanks are due to Professor Paulo Rangel Rios (EEIMVR/UFF, Brazil) for going through the manuscript meticulously.

References

[1] H.C. Rogers, Ann. Rev. Mater. Sci. 9 (1979) 283–311.
[2] K. Bitans, P.W. Whitton, Inter. Metall. Rev. 17 (1972) 66–78.
[3] S.P. Timothy, Acta Metall. 35 (1987) 301–306.
[4] S.V. Harren, H.E. Dève, J. Asaro Acta Metall. 36 (1998) 2435–2480.
[5] T.W. Wright, The Physics and Mathematics of The Adiabatic Shear Bands, Cambridge University Press, 2002.
[6] U. Andrade, K. Meyers, K.S. Vecchio, H. Chokshi, Acta Mater. 42 (1994) 3183–3195.
[7] J.A. Hines, K.S. Vecchio, Acta Mater. 45 (1997) 635–649.
[8] M.A. Meyers, U.R. Andrade, A.H. Chokshi, Metall. Mater. Trans. A 21 (1995) 2881–2893.
[9] M.A. Mogilevskii, V.V. Bulgakov, A.D. Kormachev, Combust. Explosion Shock Waves 30 (1994) 350–353.
[10] H.A. Grebe, H.-R. Pak, M.A. Meyers, Metall. Trans. A 16 (1985) 761–775.
[11] F.D.S. Marquis, Y.J. Chen, J. Phys. IV C3 (1997) 441–446.
[12] Y.J. Chen, M.A. Meyers, V.F. Nesterenko, Mater. Sci. Eng. A 268 (1999) 70–82.
[13] S. Nemat-Nasser, W. Guo, Mater. Sci. Eng. A 284 (2000) 202–210.
[14] S. Nemat-Nasser, W. Guo, Mech. Mater. 32 (2000) 243–260.
[15] M.T. Pérez-Prado, J.A. Hines, K.S. Vecchio, Acta Mater. 49 (2001) 2905–2917.
[16] M.A. Meyers, V.F. Nesterenko, J.C. Lasalvia, Y.B. Xu, Q.J. Xue, Phys. IV 9 (2000) 51–56.
[17] Y.B. Xu, W.L. Zhong, Y.J. Chen, Q. Liu, Y.L. Bai, M.A. Meyers, Mater. Sci. Eng. A 299 (2001) 287–295.
[18] C.J. Shih, V.F. Nesterenko, M.A. Meyers, J. Appl. Phys. 83 (1998) 4660–4671.
[19] M.C. Mataya, M.J. Carr, G. Krauss, Metall. Trans. A 13 (1982) 1263–1274.
[20] C.L. Wittman, M.A. Meyers, H.-R. Pak, Metall. Trans. A 21 (1999) 707–716.
[21] M.A. Meyers, C.L. Wittman, Metall. Trans. A 212 (1990) 3153–3164.
[22] C.O. Mgbokwere, S.R. Nutt, J. Duffy, Mech. Mater. 17 (1994) 97–110.
[23] M.A. Meyers, Y.B. Xu, Q. Xue, M.T. Pérez-Prado, T.R. McNelley, Acta Mater. 51 (2003) 1307–1325.
[24] G.R. Johnson, W.H. Cook, Eng. Fract. Mech. 21 (1985) 31–48.
[25] F.J. Zerilli, R.W. Armstrong, Acta Metall. Mater. 40 (1992) 1803–1808.
[26] S.R. Bodner, Y. Partom, J. Appl. Mech. 42 (1975) 385–389.
[27] P.S. Follansbe, U.F. Kocks, Acta Metall. 36 (1998) 81–93.
[28] J.A. Hines, K.S. Vecchio, S. Ahzi, Metall. Trans. A 29 (1998) 191–203.
[29] F.J. Humphreys, J. Mater. Sci. 36 (2001) 3833–3854.
[30] R.K. Ray, J.J. Jonas, Inter. Met. Rev. 39 (1994) 129–172.
[31] M. Hölscher, D. Raabe, K. Lücke, Steel Res. 62 (1991) 567–575.
[32] D. Raabe, K. Lücke, Scripta Metall. 27 (1992) 1533–1538.
[33] L.W. Meyers, S. Manwaring, in: L.W. Murr, K.P. Staudhammer, M.A. Meyers (Eds.), Metallurgical Applications of Shock-Wave and High-Strain-Rate Phenomena, Marcel Dekker, New York, 1986, pp. 657–674.
[34] A.W. Sleeswyk, Acta Metall. 10 (1962) 3803–3812.
[35] W.D. Biggs, P.L. Pratt, Acta Metall. 6 (1958) 694–703.
[36] T.C. Lindley, Acta Metall. 13 (1966) 681–689.
[37] J.N. Johnson, R.W. Rohde, J. Appl. Phys. 42 (1971) 4171–4182.
[38] J.H. Chen, G.Z. Wang, Q. Wang, Metall. Trans. A 33 (2002) 3393–3402.
[39] M.A. Meyers, G. Subhash, B.K. Kad, L. Prasad, Mech. Mater. 17 (1994) 175–193.
[40] J.F. Humphreys, M. Hatherly, Recrystalization and Related Annealing Phenomena, Pergamon Press, 1995.
[41] M.A. Meyers, Dynamic Behavior of Materials, John Wiley & Sons Inc., New York, 1984.
[42] B. Derby, Acta Metall. 39 (1991) 955–962.
[43] D. Chapelle, M. Darrieulat, Mater. Sci. Eng. A 347 (2003) 32–41.
[44] J.W. Christian, S. Mahajan, Prog. Mater. Sci. 39 (1995) 1–157.
[45] S. Mahajan, D.F. Williams, Inter. Metall. Rev. 18 (1973) 43–61.